CALIFORNIA POLYTECHNIC STATE UNIVERSITY

SAN LUIS OBISPO, CALIFORNIA 93407

Design and Evaluation of Single and Dual Flow Thrust Vector Nozzles with Post Exit Vanes

NCC2-748

(NASA-CR-193393) DESIGN AND EVALUATION OF SINGLE AND DUAL FLOW THRUST VECTOR NOZZLES WITH POST EXIT VANES Semiannual Progress Report, Jun. - Dec. 1992 (California Polytechnic State Univ.) 35 p

N94-14086

Unclas

G3/34 0186012

Semi-Annual Progress Report 6/92 - 12/92

NASA-AMES Grant Number NCC 2-748

Thomas W. Carpenter, Principle Investigator & Professor, Mechanical Engineering
Stephen E. Vaccarezza, Mechanical Engineering, Graduate Student
Sean Dobbins, Mechanical Engineering, Graduate Student

ABSTRACT

This Thrust Vectored Research project required that a 1/24 scale model of the F/A-18 High Alpha Research Vehicle, (HARV), propulsion system be constructed on the university campus. This propulsion system was designed for cold flow testing on a multicomponent test rig. Forces and moments were measured to study nozzle performance parameters. The flow visualization technique of color Schlieren photography was performed to investigate the flow phenomena at the nozzle exit. The flow interactions that were identified consisted of vane nozzleing between the outer and lower vanes and vane tip interference. The thrust vectoring system consisted of three asymmetrically spaced vanes installed circumferentially on a maximum afterburner nozzle. The performance of the nozzle was investigated with the outer and lower vanes equally deflected, (-10 deg. $< \delta_v <$ 25 deg.), and with the upper vane fully retracted, (δ_v = -10 deg.). The nozzle pressure ratio ranged from 4 to 6. The results indicated that a vane nozzleing effect developed at nozzle pressure ratios of 4 and 6 when the outer and lower vanes where deflected far enough into the flow field such that the increase in vane area accelerated the flow past the vanes causing distorted shock waves. This accelerated flow was a result of a pressure differential existing between the inside surface of the vane and the ambient pressure. The stagnation pressure that developed along the inside surface of the vane accelerated the flow past the vanes causing it to equalize with ambient pressure, thus providing distorted shock waves. A tip interference was present at the trailing edge of the upper vane as a result of low nozzle pressure, NPR 4, with high vane deflection, δ_v =25 degrees, and also with a high nozzle pressure, NPR 6, and low vane deflections, δ_v =15 degrees.

Acknowledgment

Dr. Thomas W. Carpenter, Mr. Stephen E.Vaccarezza, and Mr. Sean Dobbins want to thank Mr. James Gerhardt for the fabrication of the equipment necessary in making this such a successful and rewarding research project. His craftsmanship and meticulous attention to precise details have made it possible for us to conduct this research on the F/A-18 High Alpha Research Project.

Table of Contents

	page
Apparatus and Method	
Static Test Facility	1
Single and Dual Engine and Propulsion System	1
Nozzle Geometry	2
Vane Geometry	2
Vane Actuation System	3
Instrumentation	3
Data Reduction	4
Results and Discussion	6
Reference	8
List of Figures	ii
List of Drawings	iii
List of Photos	iv
Nomenclature	vi

List of Figures

		page
Figure 1	Coordinate system for thrust stand with forces and moments, respectively.	24
Figure 2	Sketch of jet turning angle and axial thrust loss definitions.	25

List of Drawings

		page
Drawing 1	Detail schematic of vane geometry, vane location relative to nozzle exit and vane actuation system relative to convergent nozzle. Scale 1/24.	22
Drawing 2	Schematic of left engine and post exit vane propulsion system hardware. Scale 1/24.	23

List of Photographs

		page
Photo 1	Exploded view of individual components of post exit vanes for left engine testing. Scale 1/24.	9
Photo 2	Assembled post exit vane for cold flow testing of left engine Scale 1/24.	10
Photo 3	The aft end of left engine with post exit vanes fully retracted. Scale 1/24.	11
Photo 4	Side view of post exit vanes mounted on convergent nozzle. Upper vane in full view. Vanes fully retracted. Scale 1/24.	11
Photo 5	Single engine propulsion simulation system with post exit vanes. Scale 1/24.	12
Photo 6	Manufactured components of right engine propulsion system.	13
Photo 7	Exploded view of externally pressurized bellows.	14
Photo 8	Enhanced view of externally pressurized bellows.	15
Photo 9	Enhanced view of externally pressurized bellows.	15
Photo 10	Plumbing of right and left engine propulsion simulation system.	16
Photo 11	Piping system for fully developed flow.	17
Photo 12	Pneumatic valves for regulating supply of cold compressed air to propulsion system.	18
Photo 13	Pneumatic valve control box.	18

List of Photographs (continued)

		page
Photo 14	ASME calibrated orifice plates.	19
Photo 15	Vane deflection at 0 degree NPR 4 1/24 Scale	20
Photo 16	Vane deflection at 15 degree NPR 4 1/24 Scale	20
Photo 17	Vane deflection at 25 degree NPR 4 1/24 Scale	20
Photo 18	Vane deflection at 0 degree NPR 6 1/24 Scale	21
Photo 19	Vane deflection at 15 degree NPR 6 1/24 Scale	21
Photo 20	Vane deflection at 25 degree NPR 6 1/24 Scale	21

Nomenclature

All forces and angles are referred to the model center line

F	measured thrust along body axis positive in forward direction
F_i	ideal isentropic gross thrust, lbf, $w_p \left\{ \frac{R_j T_{t,j}}{g^2} \frac{2\gamma}{(\gamma - 1)} \left[1 - \left(\frac{1}{NPR} \right)^{\frac{(\gamma-1)}{\gamma}} \right] \right\}^{\frac{1}{2}}$
F_N	measured normal force, lbf
F_r	resultant side force, lbf, $\sqrt{F^2 + F_N^2 + F_S^2}$
F_S	measured side force, lbf
g	acceleration due to gravity $1g \approx 32.174\ ft/sec^2$
p_a	ambient pressure, psia
$p_{t,j}$	average total jet pressure, psig
R_j	gas constant, 1716 ft^2/sec^2
$T_{t,j}$	jet total pressure, °R
w_i	ideal weight-flow rate, lbf/sec
w_p	measured weight flow rate, lbf./sec
γ	ratio of specific heats, 1.4 for air

$\delta_A, \delta_B, \delta_C$	geometric deflection angle of vanes at positions A, B, and C, respectively, deg
δ_P	resultant pitch thrust vector angle, $\tan^{-1}\frac{F_N}{F}$, deg
δ_y	resultant pitch thrust vector angle, $\tan^{-1}\frac{F_s}{F}$, deg
δ_v	vane deflection angle, deg

Abbreviations:

A	vane position A
(A/B)	afterburner
B	vane position B
C	vane position C
HARV	High Alpha Research Vehicle
hp	horsepower
max.	maximum
NPR	nozzle pressure ration, $p_{t,j}/p_s$

Apparatus and Method

Static Test Facility

The tests were conducted in the School of Mechanical Engineering's Engines Laboratory on the campus of California Polytechnic State University in San Luis Obispo, California. The test cell is supplied with compressed air from a 33 ft. long 5 ft. diameter air receiver tank located outside and adjacent to the testing facility.

The maximum holding capacity of compressed air was approximately 648 cubic feet. During testing, all operations of the test model propulsion system were conducted within the test cell.

The high pressure air system for the facility was maintained with clean, relatively dry ambient air compressed by a 75 hp Ingersoll-Rand compressor. The receiver tank could sustain a nozzle pressure ratio of 6, NPR 6, for approximately 60 seconds for single engine testing,[Reference. 1].

Single and Dual Engine Propulsion Systems

Photos 1, 2 indicate the assembly of one large vane and two standard vanes for the left engine. The nozzle was designed to 1/24 scale of the maximum (A/B) nozzle specifications, [Reference. 2]. Photos 3, 4 indicate the aft end and side view of the left engine with three post exit vanes. The completed assembly of the scale model propulsion system for the left engine is indicated in Photo 5.

Completion of the right engine and post exit vanes is scheduled for early summer of 1993. The assembled components of the right engine that have been machined included: (1) the plenum (2) externally pressurized bellows, and (3) converging nozzle as indicated in Photos 6 and 7. The converging nozzle and vane assembly for the right engine are identical to the left engine as shown by Photos 1 and 3.

The externally pressurized bellows configuration in Photos 7, 8, and 9 were designed to operate under tension with pressure ranges up to 6 NPR. The bellows assembly minimize the transmission of unwanted forces to the thrust stand and provide a linearization with pressure of those forces that are transmitted. This allows the elimination of the unwanted forces through calibration.

The plumbing of the air supply for the right engine to the test rig has been completed as indicated in Photo 10.

The test cell air supply line was plumbed in such a manner as to provide fully developed flow conditions upstream of the flow measurement orifice plate, see Photo 11. The air supplied to the flow nozzles was controlled with 2 inch ball valves pneumatically operated. The air was supplied to a plenum attached to the base of the nozzle to insure steady flow at the entrance of the nozzle. The nozzle base was bolted to the top of the test rig. It was from this design that the propulsion system was calibrated and the left engine tested with post exit vanes.

Nozzle Geometry

The nozzle design used in this experiment was a 1/24 scale model of a F/A-18 convergent nozzle. The nozzle configuration for this test represented a maximum (A/B)-power setting. Details of the nozzle geometry are given in Drawings 1 and 2 and Reference 2.

Vane Geometry

The three vane vectoring geometry reported in Reference 2 provided the basis for the 1/24 scale model vane design. The vane design consisted of three vanes- the upper, the outer, and the lower vane, which were placed on the converging nozzle according to the specifications of Reference 2 and Drawing 1. The outer and lower vanes were referred to as the *standard* vane and the upper vane was referred to as the *large* vane.

Each vane was designed with double curvature, on the vane surface. The areas for the standard vanes and large vane were 0.413 in^2 and 0.579 in^2, respectively. The larger vane surface area was approximately 29 percent greater then the standard vane surface area.

The corners of the vanes where trimmed at the trailing edge. This was a design specified in Reference 2 and allowed for complete closure of any two vanes at angles of 35 degrees, without physical interference between vanes. During testing, two vanes where deflected into the jet while the third remained fully retracted (out of the jet flow at -10 degrees).

Vane Actuation System

Drawings of the vane linkage system are provided as Drawings 1,2. The vanes were mounted to the vane linkage shown in Drawing 1 by two set screws. The linkage was carefully welded to the outside surface of the converging nozzle. The vane was allowed to rotate through the slotted curve while pivoting on the vane linkage. The arrangement of the curved slot and pivot point on the linkage allowed the vanes to rotate from -10 degrees through 30 degrees. The maximum vane deflection tested for in this experiment was 25 degrees.

When the vane deflection angle was set for each vane, a set of precision cut blocks with angle inclinations varying from -10 through 25 degrees was used to verify the actual inclination.

Drawing 1 shows the orientation of the three vanes at the exit plane of the converging nozzle. The three thrust vectoring vanes were arranged circumferentially about the nozzle exit exactly as the full scale vanes tested on the F/A-18 HARV. The upper vane, (vane A), was located 5 degrees clockwise from the vertical centerline of the nozzle. The outer vane, (vane B), was located 118.0 degrees counterclockwise from the mounting point of vane A. The lower vane, (vane C), was located 138.5 degrees clockwise from the mounting point of vane A.

Instrumentation

The six component load cell test rig was used to measure forces and moments. The total pressure was measured at various locations by pressure transducers upstream and downstream of the pneumatic valve. This pneumatic ball valve was used to control the pressure in the plenum and nozzle by adjusting a needle screw at the pneumatic valve control box, see Photo 12 and Photo 13.

The weight flow rates were measured from pressure and temperature measurements taken at the Daniel Orifice plate [Reference 3], see Photo 14.

The total nozzle pressure was computed as the average of individual total pressures taken over a time period at the plenum. This average consisted of a minimum sample population of 30.

A data acquisition system sampled the pressure transducers, thermocouples, and load cells. This information was then down loaded to a personal computer

and the data was manipulated through a series of built-in macros in a spreadsheet software program.

Data Reduction

The data acquisition system sampled 10 channels every 1.5 seconds for a specific nozzle pressure until the air receiver could no longer deliver the required supply pressure to the test rig. The time required to exhaust the air supply varied with nozzle pressure, however for an NPR of 5 the air supply could hold the required pressure for greater than a minute. The averaged values were used in all subsequent computations. The multicomponent test rig with a coordinate system indicated by Figure 1, used 250 lb. load cells measured along the axis of the nozzle, (i.e., the z direction). Normal and side forces (i.e., x and y direction) were measured with 25 lb. load cells. Each of the three load cells measuring forces along the axis of the nozzle was calibrated and initially corrected for tare weight. The axial thrust direction of the test rig, at a confidence level of 95 percent, was determined through calibration to be accurate to ± 0.3125 lbf. for the most extreme range of axial loading conditions, see Reference 4.

Five computed performance parameters were used to evaluate the performance of the nozzle and were selected from Reference 5. These parameters were, internal thrust ratio F/F_i, resultant thrust ratio F_r/F_i, discharge coefficient w_p/w_i, resultant pitch vector angle δ_p, and resultant yaw vector angle δ_y. All data (i.e., thrust parameters and vector angles) were referenced to the model centerline.

Internal thrust ratio F_r/F_i was the ratio of the measured nozzle thrust along the body axis to the ideal isentropic gross thrust of the nozzle. The nozzle internal thrust F was equivalent to the fully corrected axial force measured by the six component test rig. The ideal thrust F_i was computed per Reference 5.

The resultant thrust ratio F_r/F_i was the ratio of the nozzle resultant gross thrust F_r to the ideal thrust F_i. The resultant thrust was computed from the fully corrected balance measurements of the axial-force, normal-force, and the side-force components of the jet resultant force.

The nozzle discharge coefficient wp/w_i was the ratio of the measured weight-flow rate to the ideal weight-flow rate.

The resultant thrust vector angles reflected the degree of the actual jet-flow deflection away from the axial direction. The resultant pitch vector angle δ_p was computed from the axial-force and normal force; the resultant yaw vector angle δ_y was computed from the axial-force and side force measurements.

Results and Discussions

The tests that were performed on the left engine with post exit vanes involved equal deflection of the outer and lower vanes and a fully retracted upper vane. Initially, all three vanes were set at a -10 degrees. During testing the upper vane remained at -10 degree while the outer vane and lower vane were equally deflected into the flow. This testing arrangement were conducted for nozzle pressures ratios of 3, 4 and 5, respectively.

The test rig used in this experimental work made it possible to investigate, through flow visualization techniques, the actual flow phenomena occurring between the vanes. The technique included a high energy light source, two spherical mirrors, and color filters. This method is known as the Schlieren technique.

As the nozzle pressure ratio increases the outer boundaries of the plume also increased. At a NPR 4 it was found through Schlieren photographs that the upper vane had no contact with the plume until the outer and lower vanes were fully deflected into the flow at 25 degrees. The upper vane interference was noted at the tip of the trailing edge of the vane. What had an additional impact at NPR 4 was not the increase in plume size nor straightening effect of the upper vane tip but rather the visible amount of vane nozzleing developing between the outer and lower vanes. This vane nozzleing was seen as the velocity of the air accelerating between the outer and lower vanes casuing distorted shock waves to appear in the color Schlieren photographes, see Photos 16 and 17.

The equally deflected vanes at NPR 4 began to show vane nozzleing at 5 degrees. At vane deflection of 15 degrees an accelerated air flow developed between the outer and lower vanes causing a nozzleing phenomena. This vane setting provided clear evidence that no straightening effect nor tip effect of the trailing edge by the upper vane had developed, see Photo 16. In addition, the vane deflection at 25 degrees had increased the vane nozzleing and total plume distortion. The distorted shock waves at 25 degrees had increased in strength due to the presence of more surface vane area in the flow field. This increase in vane area contributed to the accelerated flow between the vanes.

The nozzle pressure ratio of 6 that was investigated on this test rig indicate an early development of plume distortion. It is evident that from Photo 18 that the outer boundaries of the plume had begun to contact the full surface area of the upper vane.

Photo 19 indicates vane nozzleing at a vane deflection of 15 degrees with full plume distortion. The high pressure ratio contacted the vane area of the outer and lower vane resulting in the accelerate flow past the vanes. The oblique shock was present at the trailing edge of the deflected vanes. The plume made complete contact with the upper vane and tip effect of the trailing edge upper vane was present.

Photo 20 indicates evidence of strong distorted shock waves and a tip effect at the trailing edge of the upper vane. At this nozzle pressure ratio of 6 the outer and lower vanes were set at 25 degrees into the flow. An increase in vane area in the direction of flow produced a strong presence of distorted shock waves. The 25 degree vane setting also helped to turn the flow in the direction of the upper vane causing a tip effect.

The straightening effect of the upper vane was a valid assumption, per reference 2, since photo 17 indicated the only contact of the exhaust plume with the vane was at the tip of the trailing edge. The plume contact at the tip of the trailing edge of the vane for NPR 4 are large enough to increase the axial force. However, vane nozzleing does increase the loss in thrust efficiency due to the accelerated flow past the outer and lower vanes.

Schlieren photos for NPR 6 indicate a possible increase in axial force by the tip effect of the upper vane. The vane nozzleing, between the outer and lower vanes and the tip effect at the upper vane, for a vane deflection of 25 degrees indicated a potential loss in thrust efficiency.

References

1. Semi Annual Progress Report 1/92-6/92
   NASA-AMES Grant Number NCC 2-748

2. Bowers, Albion H., Noffz, Gregory K.; Grafton, Sue B.; Mason, Mary L.; Peron, Lee R; Multiaxis Thrust Vectoring Using Axisymmetric Nozzles and Postexit Vanes on an F/A-18 Configuration Vehicle;
   April 1991

3. ASME Standard; Measurement of Fluid Flow in Pipes Using Orifice, Nozzle, and Venturi; MFC-3M-1985

4. Davis, Mark; Analysis of Single Flow with Post Exit Vanes on a Multicomponent Thrust Stand; California Polytechnic State University, San Luis Obispo, Ca; 1993

5. NASA Technical Memorandum 4359
   June 1992

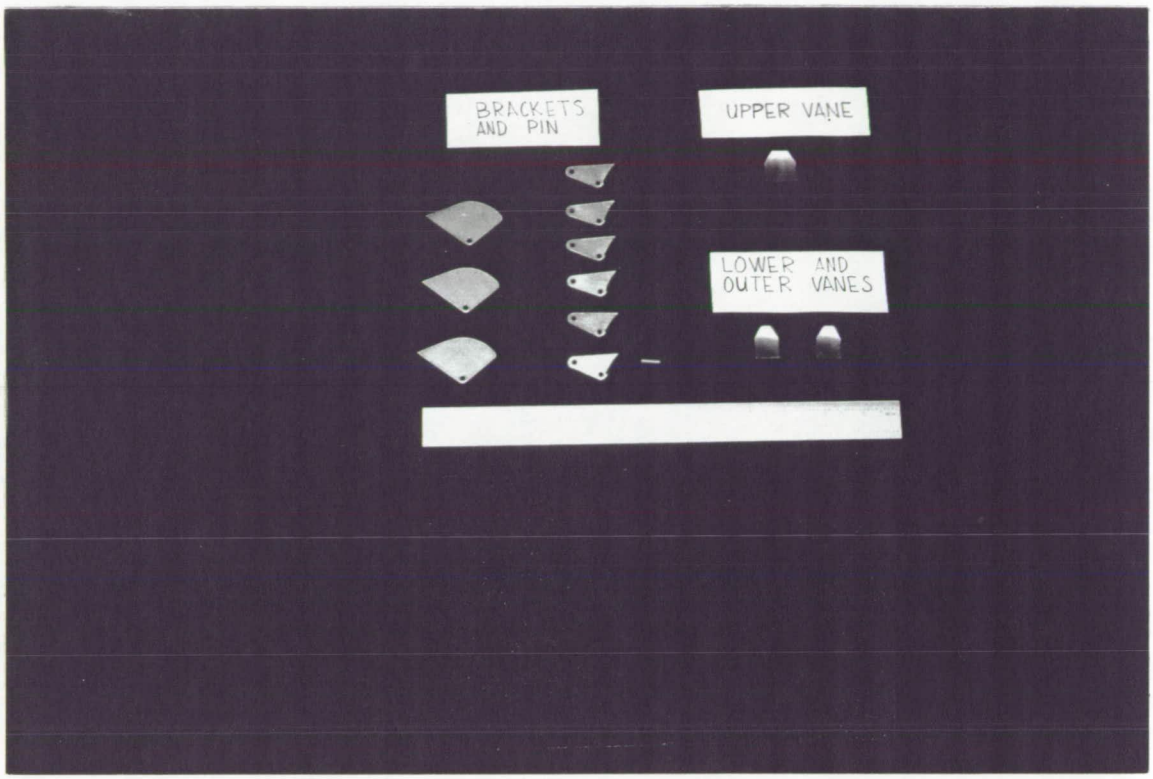

Photo 1 Exploded view of individual components of post exit vanes for left engine testing. Scale 1/24.

ORIGINAL PAGE
COLOR PHOTOGRAPH

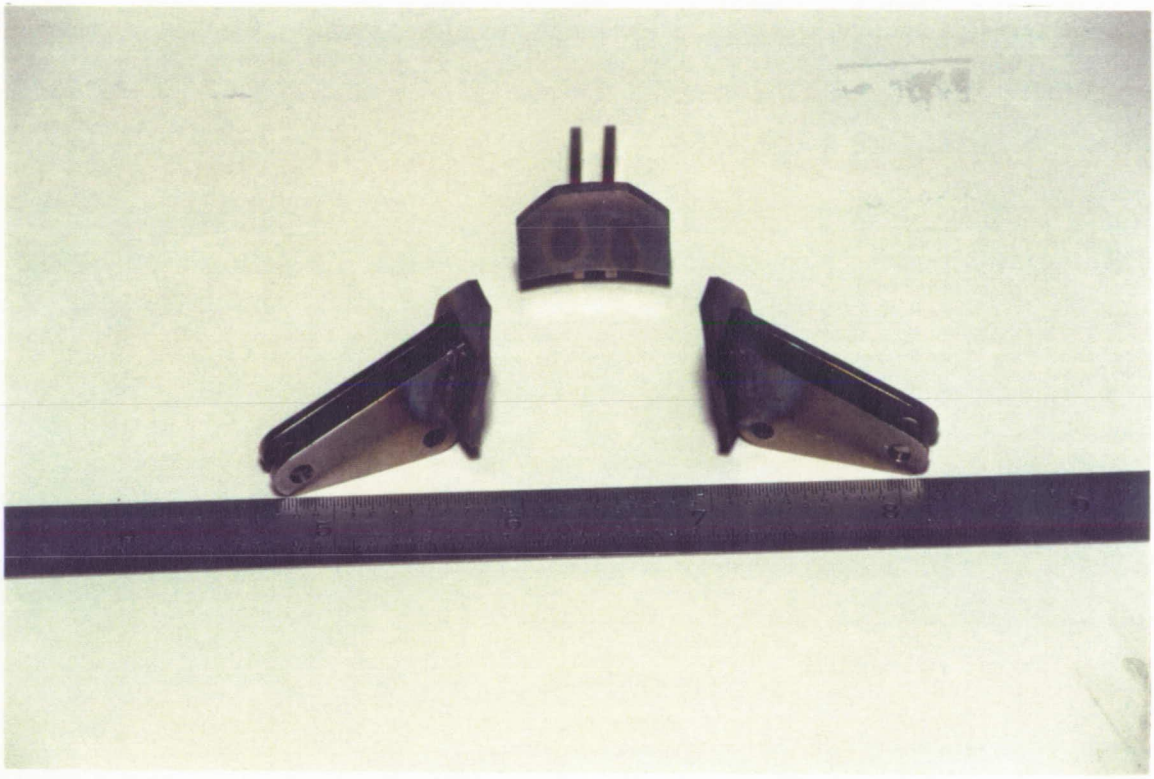

Photo 2 Assembled post exit vane for cold flow testing of left engine Scale 1/24.

ORIGINAL PAGE
COLOR PHOTOGRAPH

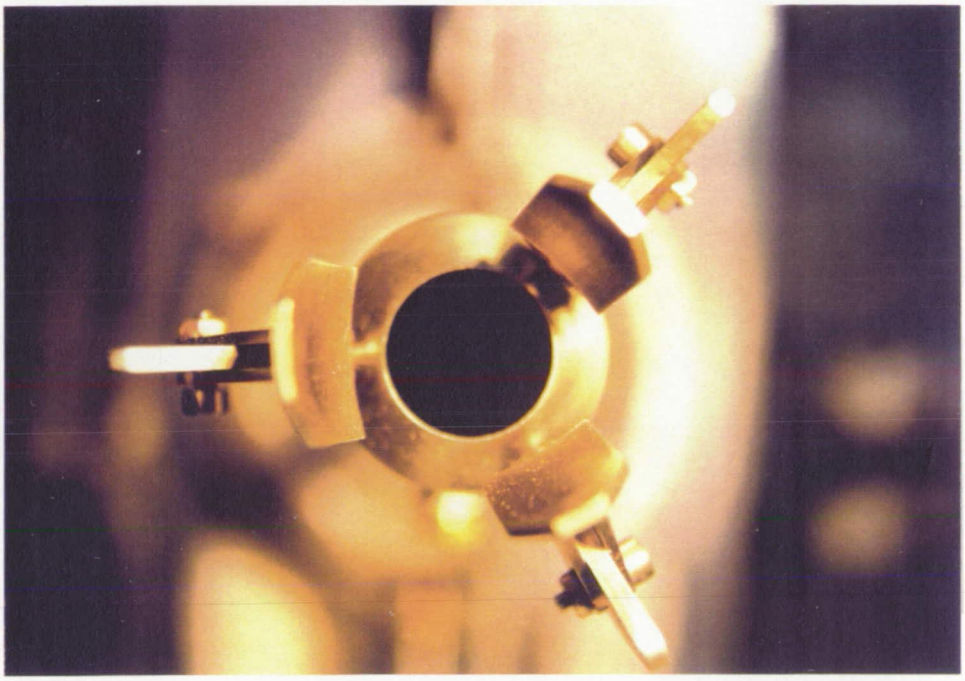

Photo 3 The aft end of left engine with post exit vanes fully retracted. Scale 1/24

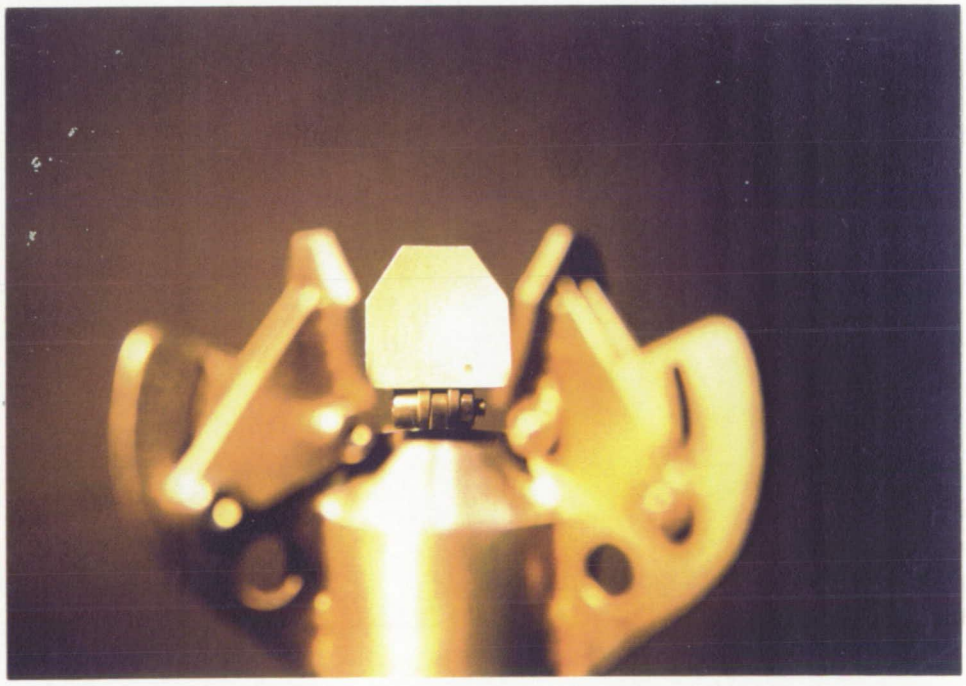

Photo 4 Side view of post exit vanes mounted on convergent nozzle. Upper vane in full view. Vanes fully retracted. Scale 1/24.

ORIGINAL PAGE
COLOR PHOTOGRAPH

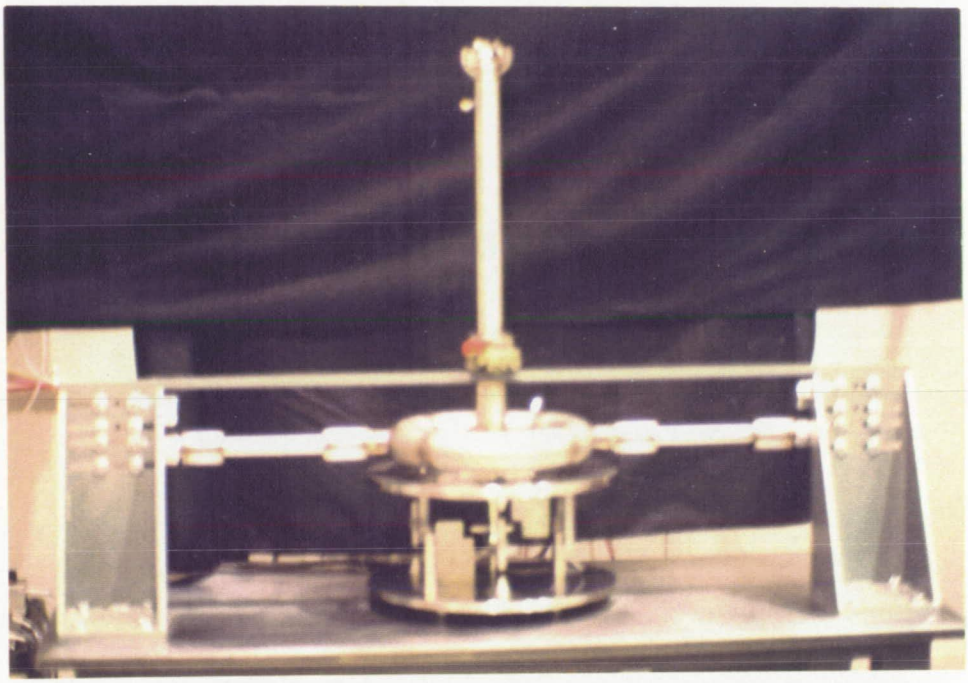

Photo 5 Single engine propulsion simulation system with post exit vanes. Scale 1/24

ORIGINAL PAGE
COLOR PHOTOGRAPH

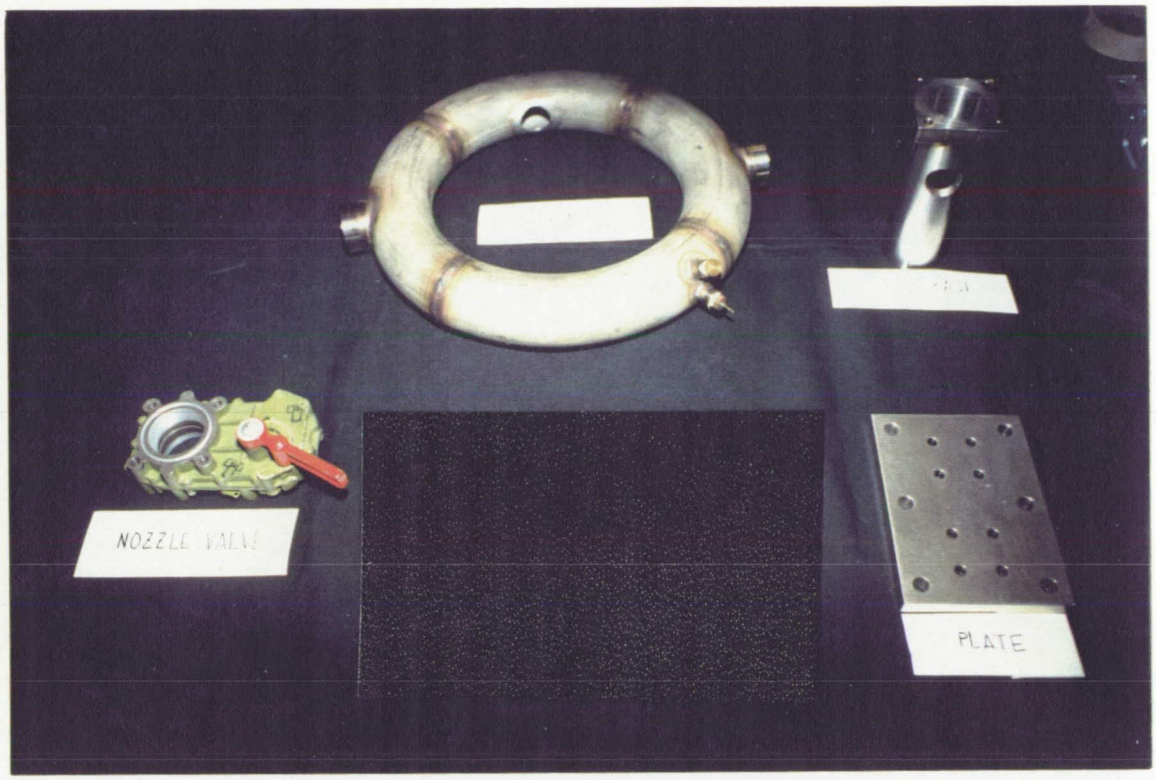

Photo 6 Manufactured components of right engine propulsion system.

ORIGINAL PAGE
COLOR PHOTOGRAPH

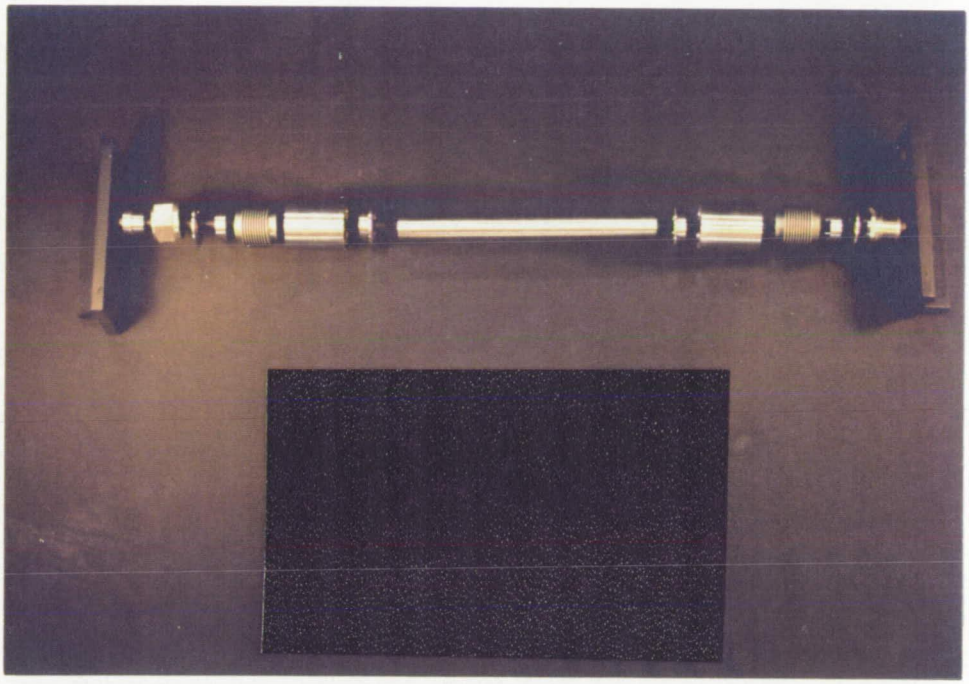

Photo 7 Exploded view of externally pressurized bellow.

ORIGINAL PAGE
COLOR PHOTOGRAPH

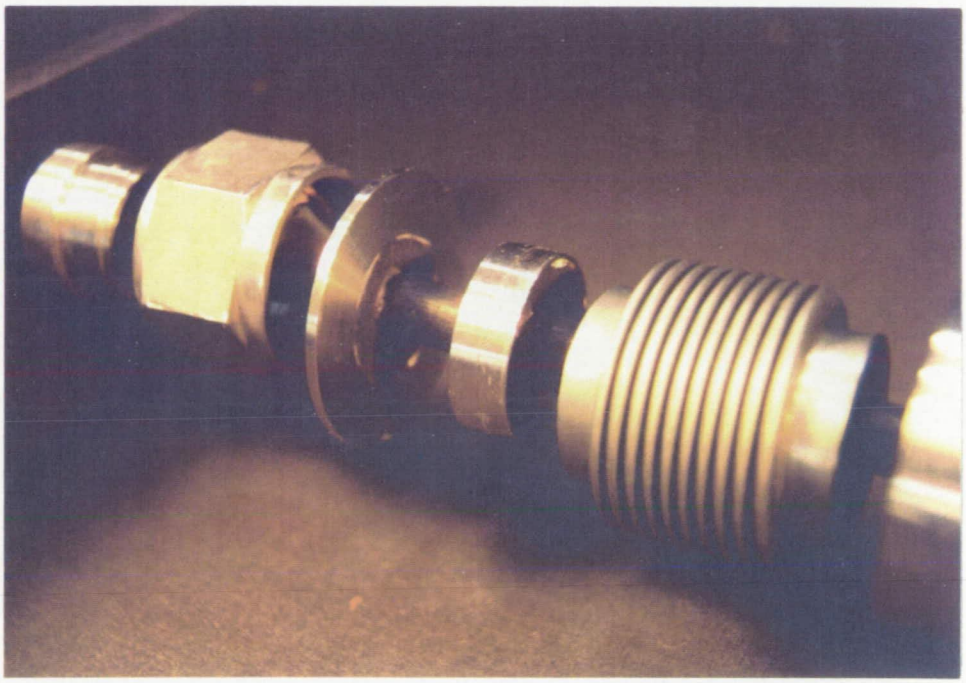

Photo 8 Enhanced view of externally pressurized bellow.

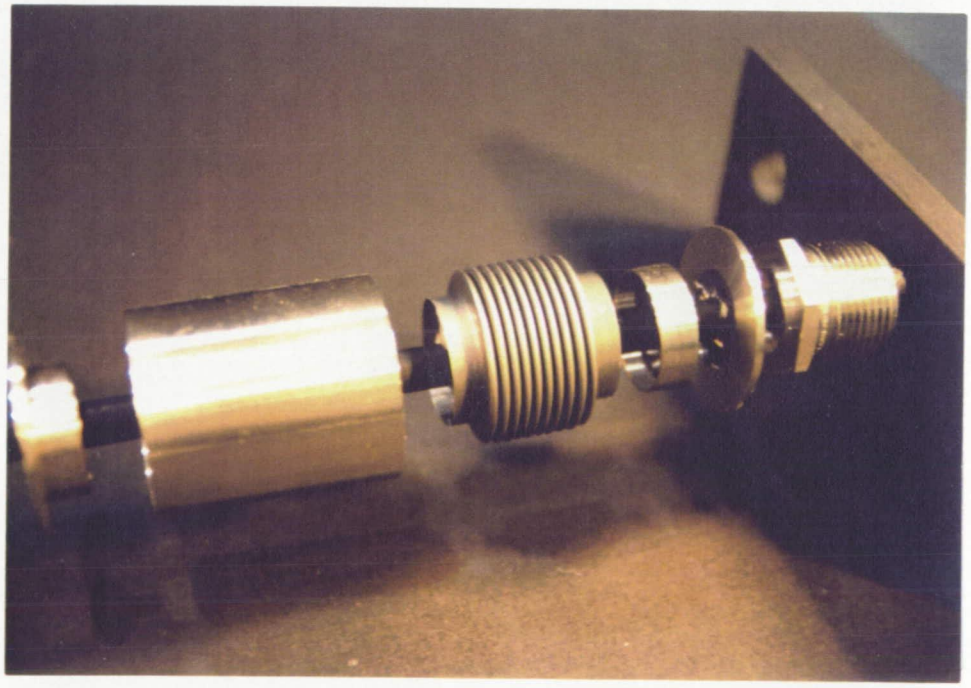

Photo 9 Enhanced view of externally pressurized bellow.

ORIGINAL PAGE
COLOR PHOTOGRAPH

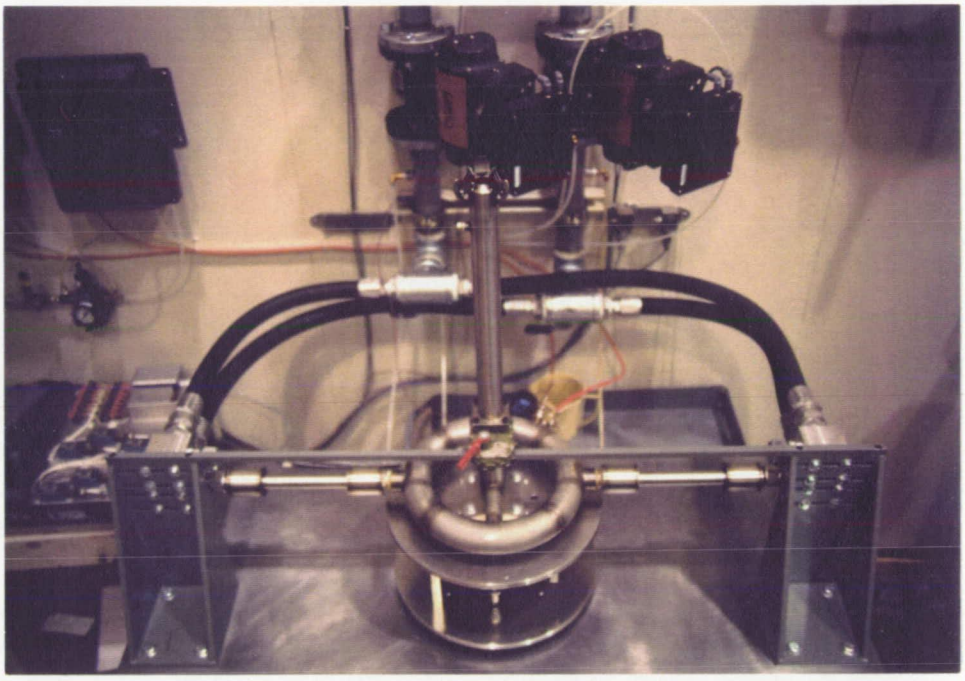

Photo 10 Plumbing of right and left engine propulsion simulation system.

ORIGINAL PAGE
COLOR PHOTOGRAPH

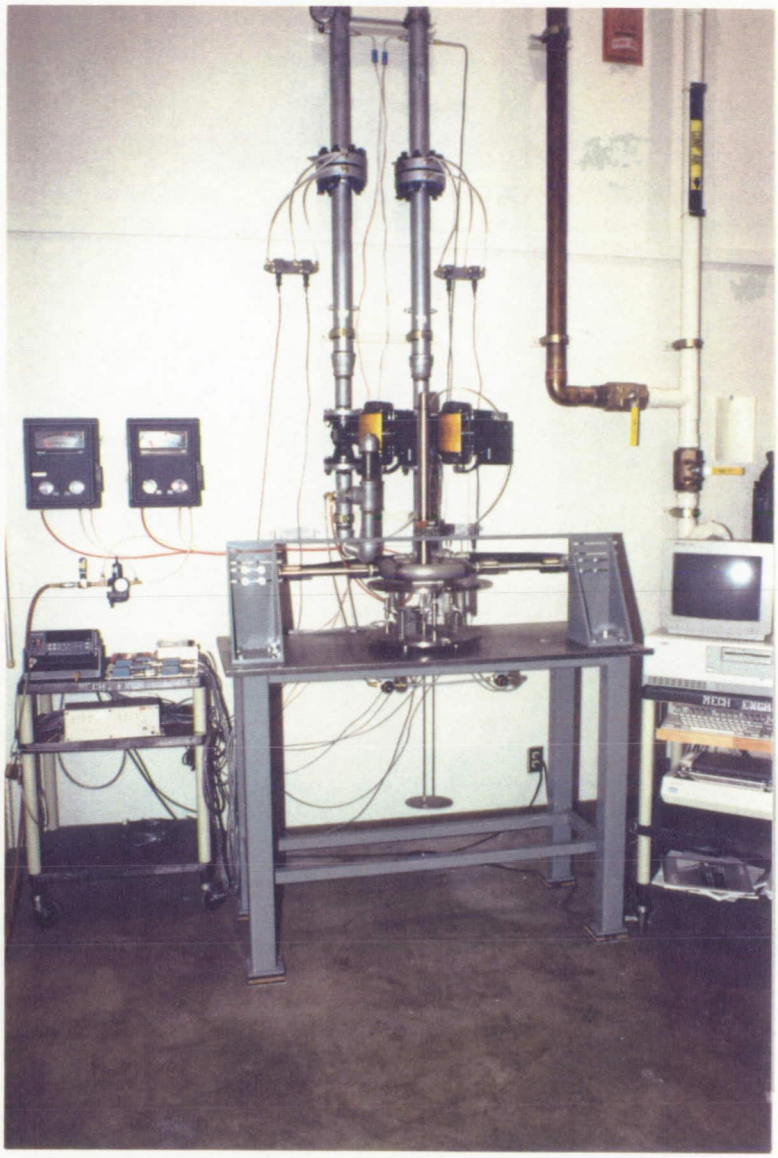

Photo 11 Piping system for fully developed flow.

ORIGINAL PAGE
COLOR PHOTOGRAPH

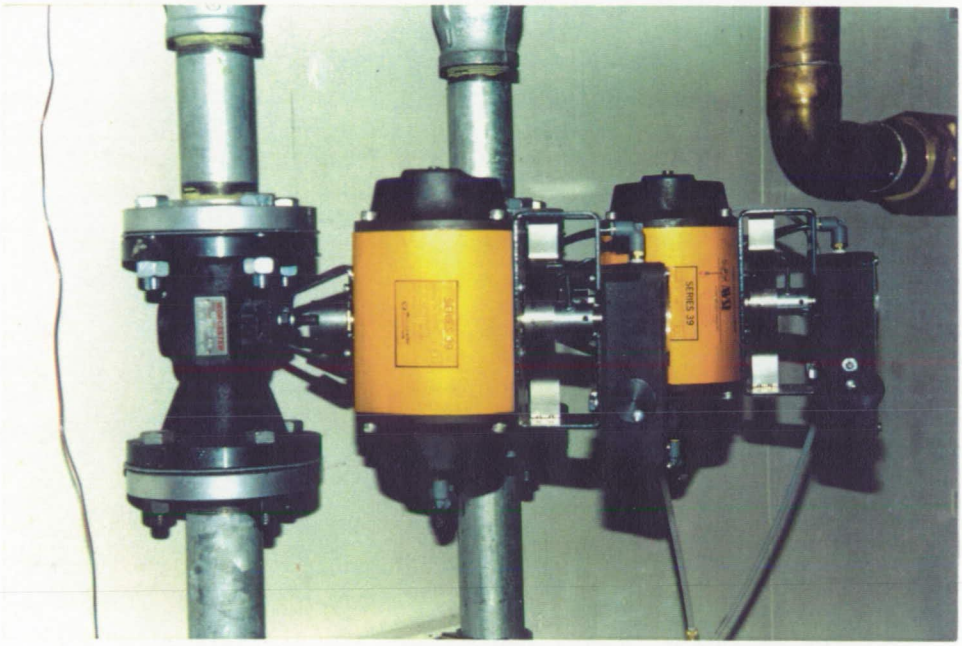

Photo 12 Pneumatic valves for regulating supply of cold compressed air to propulsion system.

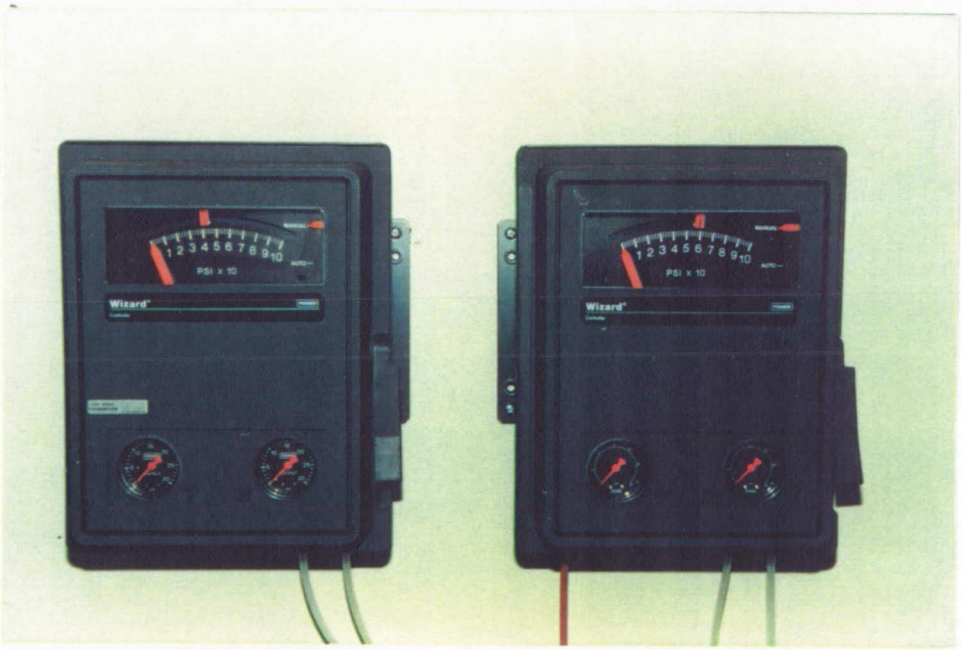

Photo 13 Pneumatic valve control box.

ORIGINAL PAGE
COLOR PHOTOGRAPH

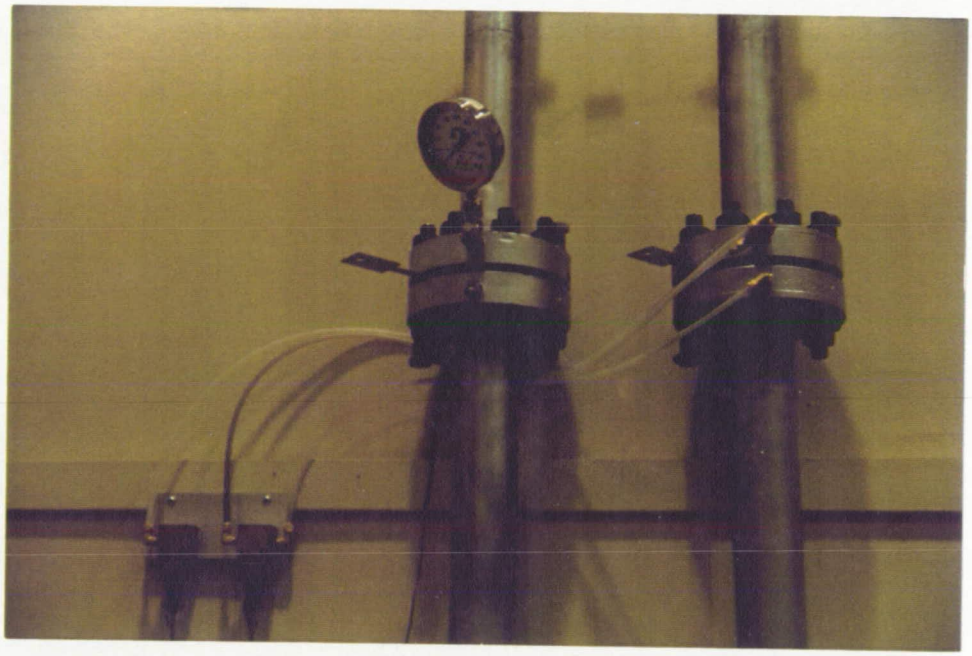

Photo 14 ASME calibrated orifice plates.

Photo 15 Vane deflection at 0 degree
NPR 4 1/24 Scale

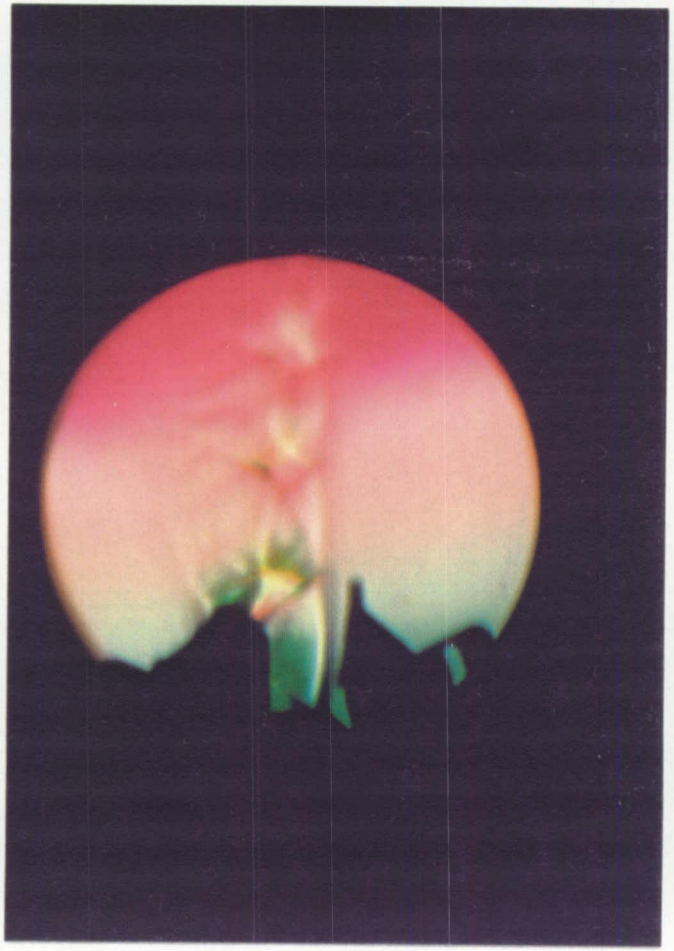

Photo 16 Vane deflection at 15 degree
NPR 4 1/24 Scale

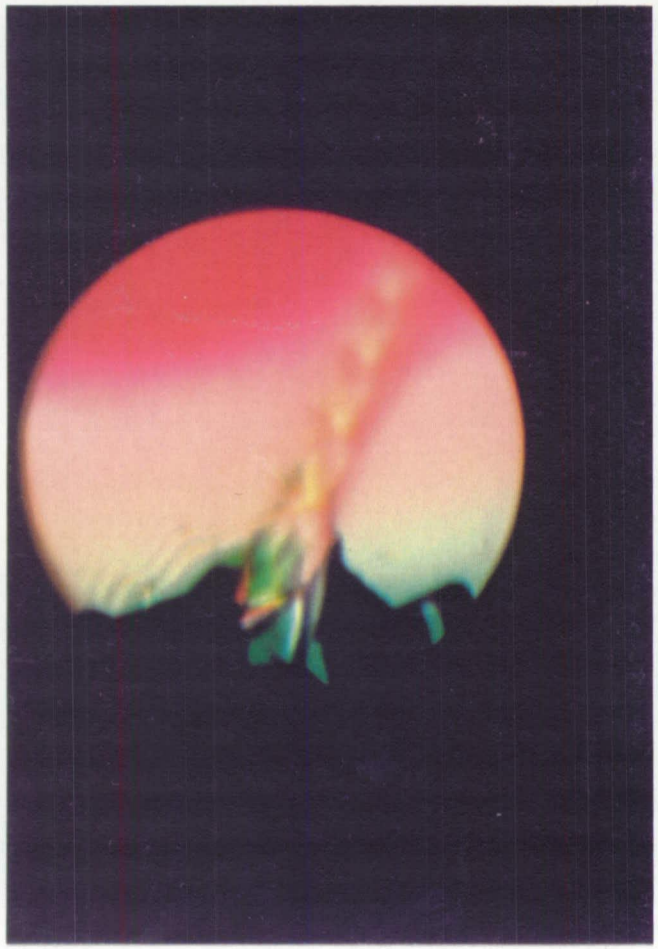

Photo 17 Vane deflection at 25 degree
NPR 4 1/24 Scale

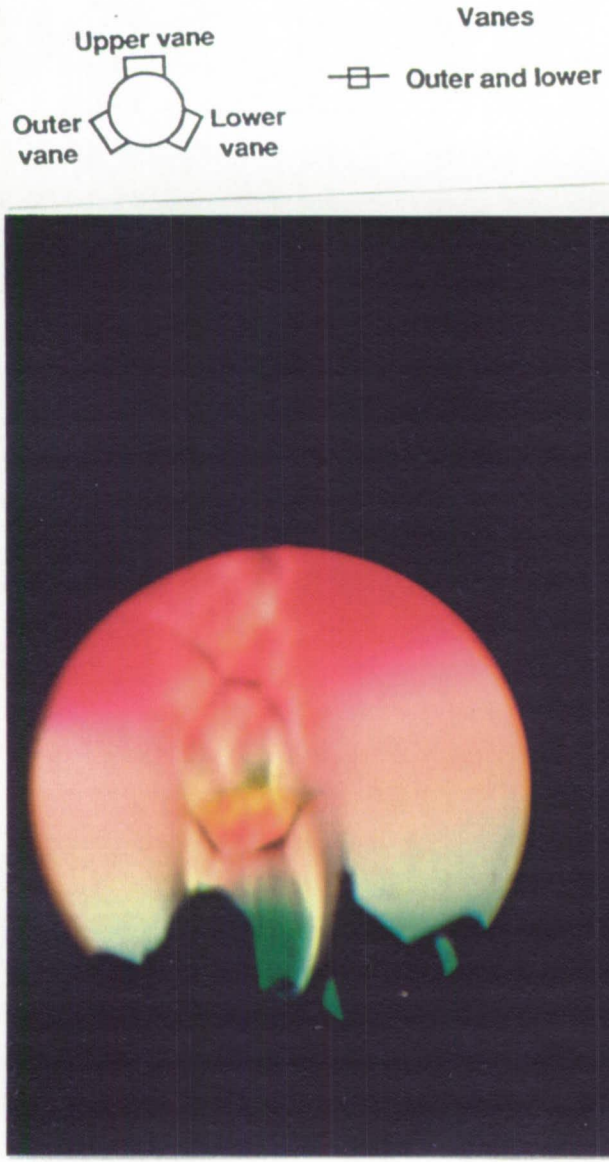

Photo 18 Vane deflection at 0 degree
NPR 6 1/24 Scale

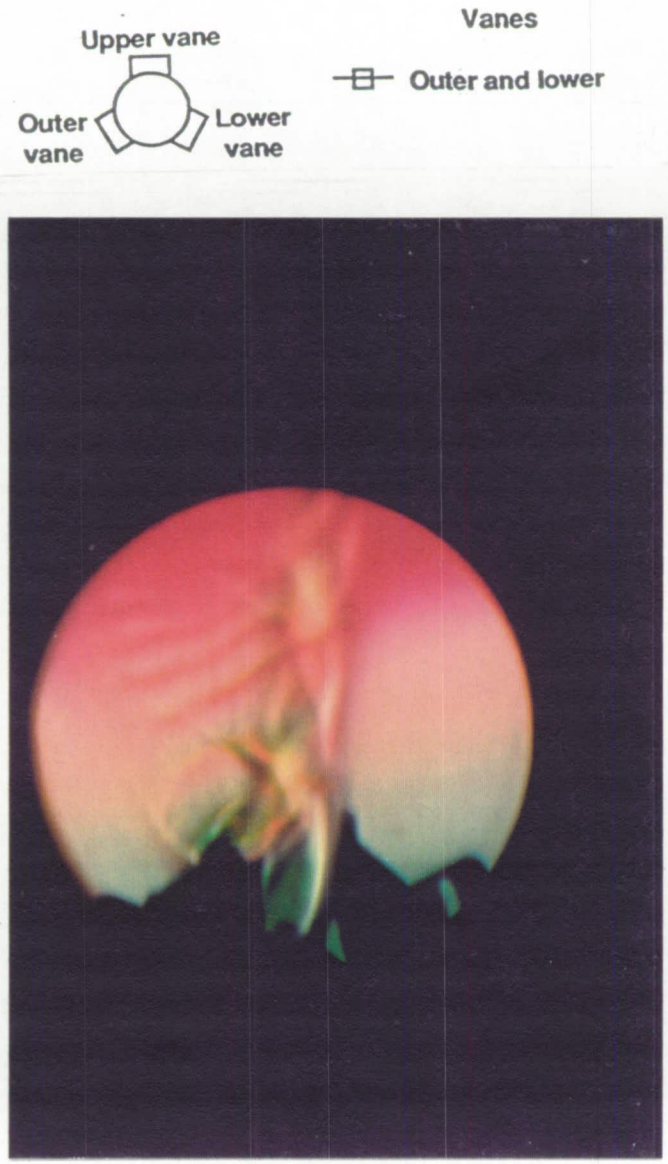

Photo 19 Vane deflection at 15 degree
NPR 6 1/24 Scale

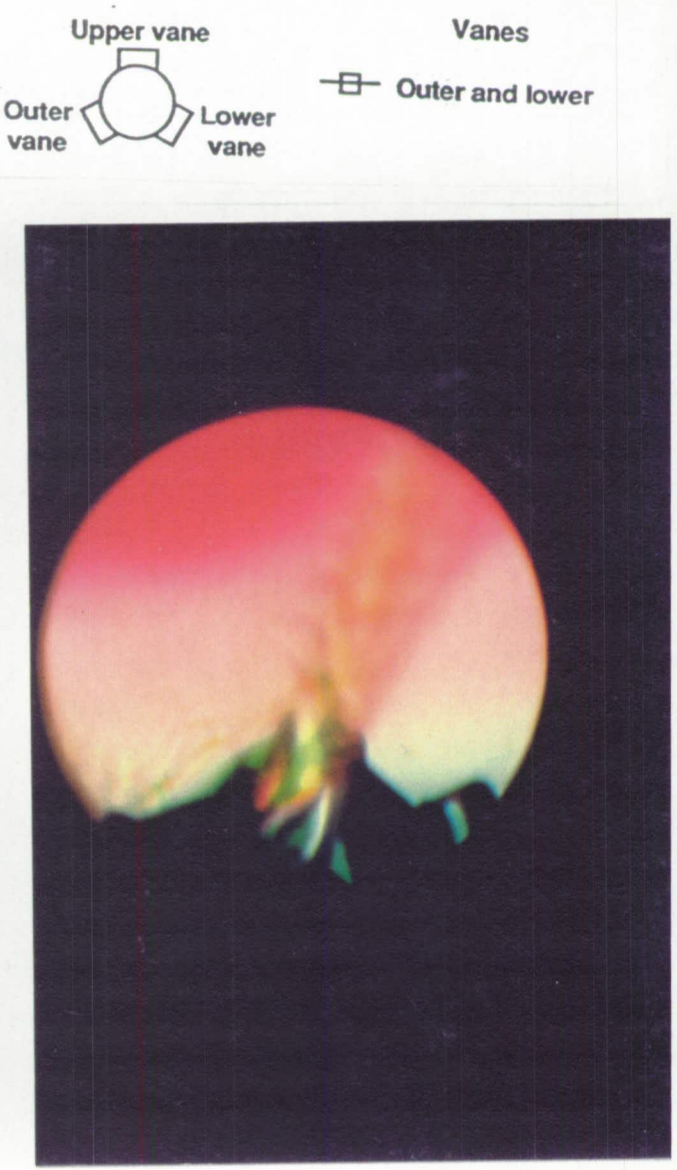

Photo 20 Vane deflection at 25 degree
NPR 6 1/24 Scale

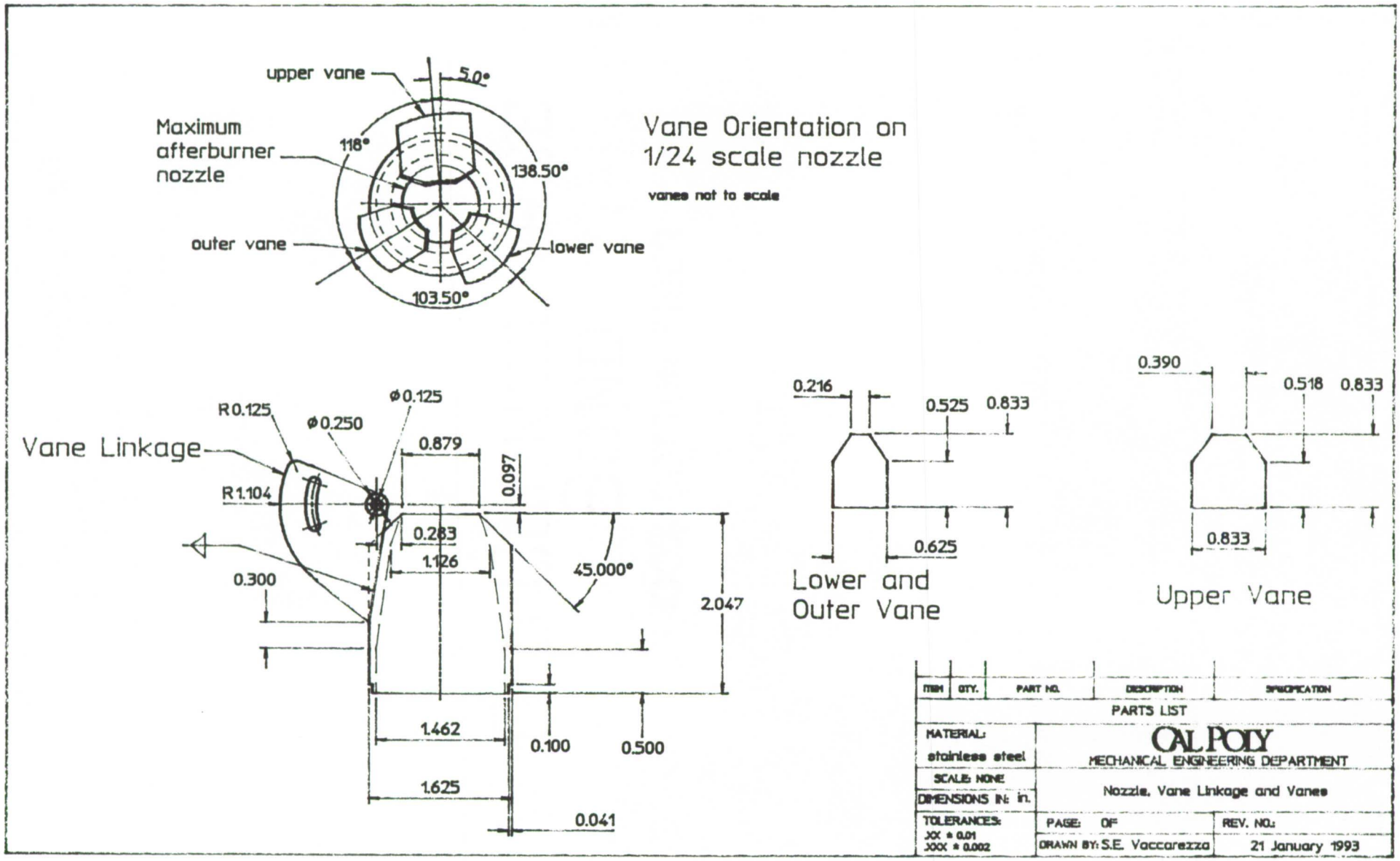

Drawing 1 Detail schematic of vane geometry, vane location relative to nozzle exit and vane actuation system relative to convergent nozzle. Scale 1/24

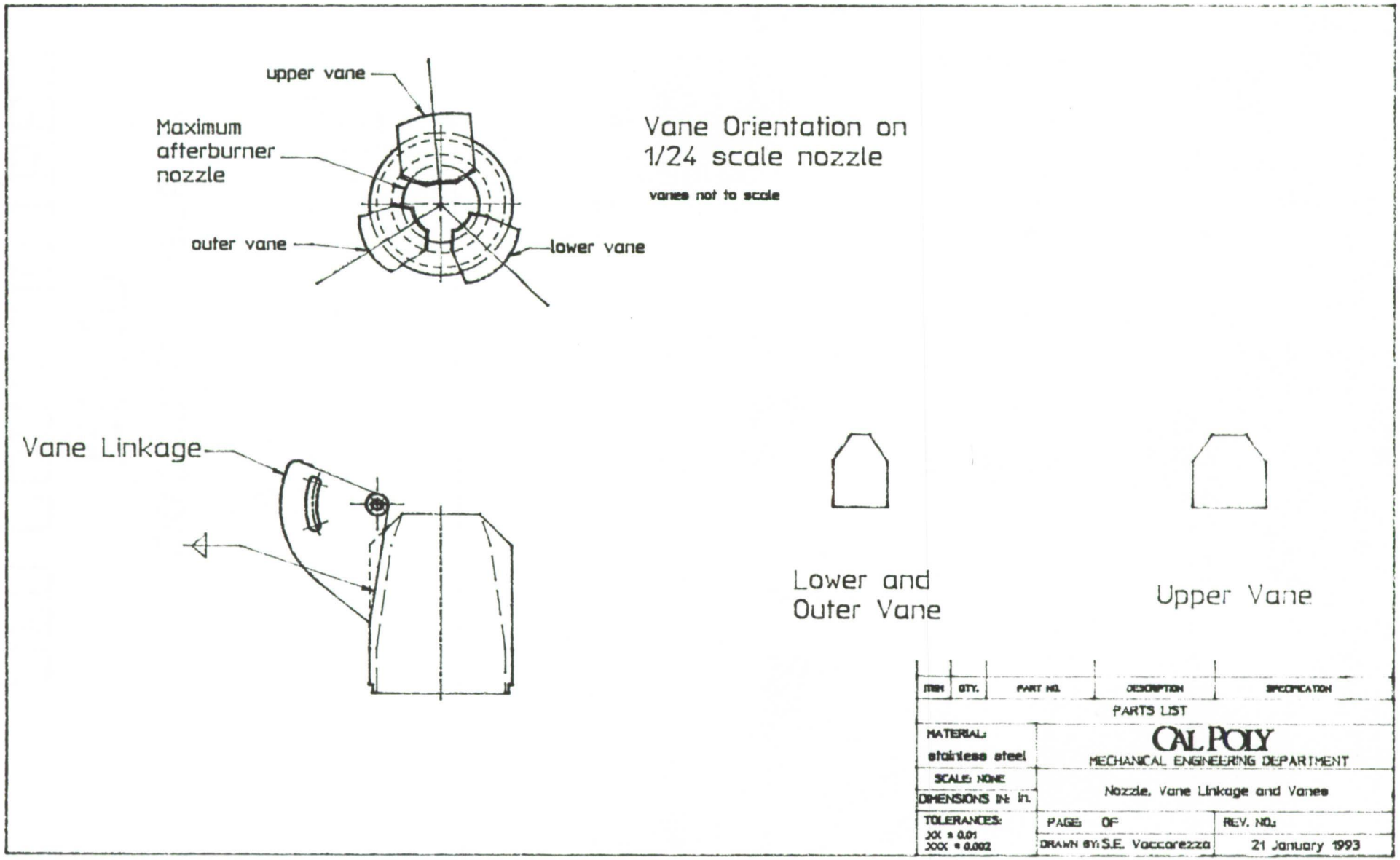

Drawing 2 Schematic of left engine and post exit vane propulsion system hardware. Scale 1/24.

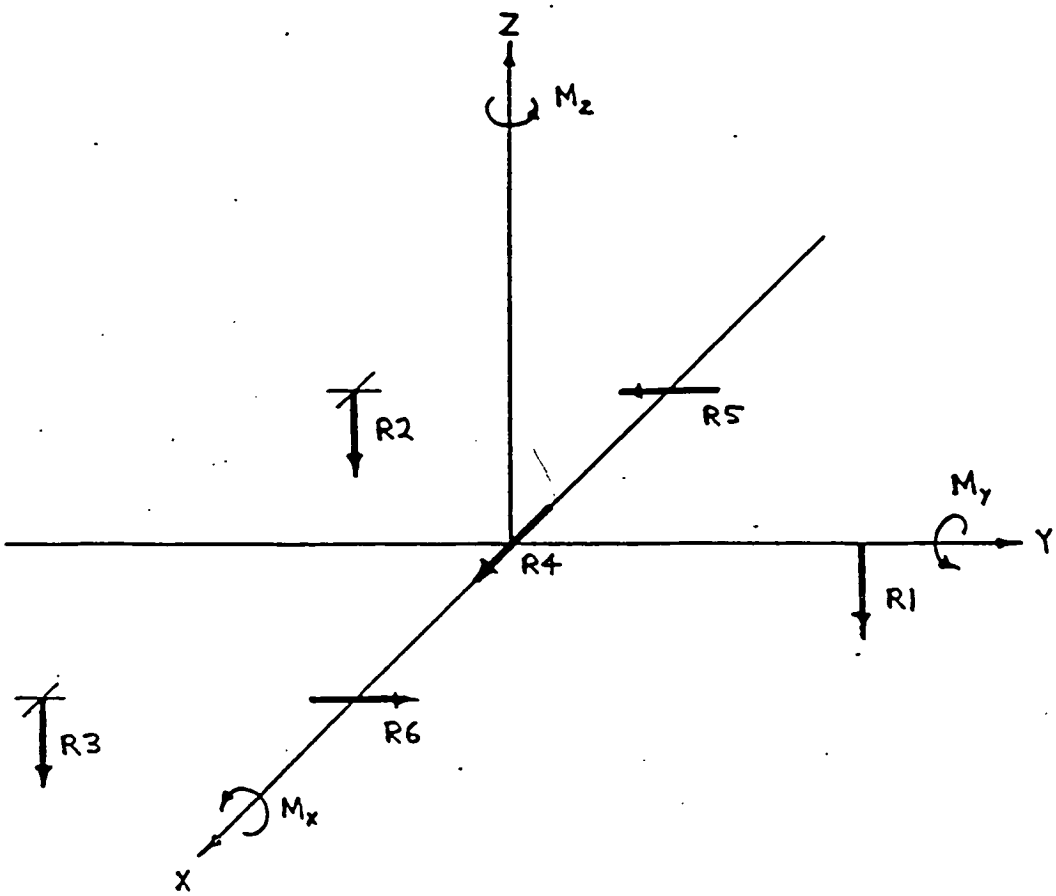

Figure 1 Coordinate system for thrust stand with forces and moments, respectively.

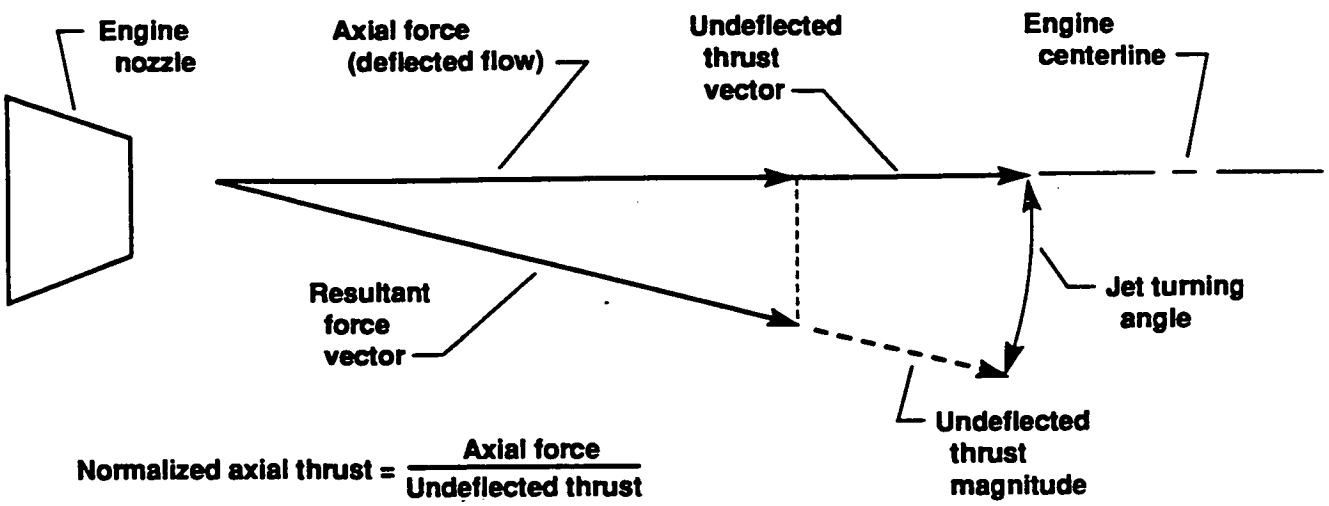

Figure 2 Sketch of jet turning angle and axial thrust loss definitions.